The Porcine Cyclic GMP-AMP Synthase-STING Pathway Exerts an Unusual Antiviral Function Independent of Interferon and Autophagy

Sen Jiang, Nengwen Xia, Jia Luo, Youwen Zhang, Qi Cao, Jiajia Zhang, Yuening Wang, Yuan Zhao, Wanglong Zheng, Nanhua Chen, et al.

▶ **To cite this version:**

Sen Jiang, Nengwen Xia, Jia Luo, Youwen Zhang, Qi Cao, et al.. The Porcine Cyclic GMP-AMP Synthase-STING Pathway Exerts an Unusual Antiviral Function Independent of Interferon and Autophagy. Journal of Virology, 2022, 96 (23), pp.e0147622. 10.1128/jvi.01476-22 . hal-04050238

HAL Id: hal-04050238
https://hal.inrae.fr/hal-04050238

Submitted on 21 Mar 2024

HAL is a multi-disciplinary open access archive for the deposit and dissemination of scientific research documents, whether they are published or not. The documents may come from teaching and research institutions in France or abroad, or from public or private research centers.

L'archive ouverte pluridisciplinaire **HAL**, est destinée au dépôt et à la diffusion de documents scientifiques de niveau recherche, publiés ou non, émanant des établissements d'enseignement et de recherche français ou étrangers, des laboratoires publics ou privés.

Distributed under a Creative Commons Attribution 4.0 International License

Journal of Virology®

CELLULAR RESPONSE TO INFECTION

The Porcine Cyclic GMP-AMP Synthase-STING Pathway Exerts an Unusual Antiviral Function Independent of Interferon and Autophagy

Sen Jiang,[a,b,c,d] Nengwen Xia,[a,b,c,d] Jia Luo,[a,b,c,d] Youwen Zhang,[a,b,c,d] Qi Cao,[a,b,c,d] Jiajia Zhang,[a,b,c,d] Yuening Wang,[a,b,c,d] Yuan Zhao,[a,b,c,d] Wanglong Zheng,[a,b,c,d] Nanhua Chen,[a,b,c,d] François Meurens,[e,f] Xiangdong Li,[a,b,c,d] Jianzhong Zhu[a,b,c,d]

[a]Comparative Medicine Research Institute, Yangzhou University, Yangzhou, China
[b]College of Veterinary Medicine, Yangzhou University, Yangzhou, China
[c]Joint International Research Laboratory of Agriculture and Agri-Product Safety, Yangzhou, China
[d]Jiangsu Co-innovation Center for Prevention and Control of Important Animal Infectious Diseases and Zoonoses, Yangzhou University, Yangzhou, China
[e]BIOEPAR, INRAE, ONIRIS, Nantes, France
[f]Department of Veterinary Microbiology and Immunology, Western College of Veterinary Medicine, University of Saskatchewan, Saskatoon, Canada

ABSTRACT The innate immune DNA-sensing cyclic GMP-AMP synthase (cGAS)-stimulator of interferon (IFN) gene (STING) pathway exerts strong antiviral activity through downstream IFN production; however, it has been recently recognized that an IFN-independent activity of STING also plays an important role in antiviral functions. Nevertheless, the IFN-independent antiviral activity of STING is not fully understood. Here, we showed that porcine STING (pSTING) played a critical role against herpes simplex virus 1 (HSV-1) and vesicular stomatitis virus (VSV) infections, and IFN-defective mutants, including pSTING pLxIS sub, S365A, and △CTT, all exhibited similar antiviral functions, compared to wild-type (WT) pSTING. Furthermore, all of these IFN-defective pSTING mutants possessed comparable autophagy activity, relative to WT pSTING, as expected. From pSTING WT, S365A, and △CTT, the residues responsible for autophagy, including L333A/R334A, Y167A/L170A, and Y245A/L248A, were mutated. Surprisingly, all of these autophagy-defective pSTING mutants still resisted the two viral infections, demonstrating that the pSTING antiviral function is independent of IFN as well as autophagy. On the other hand, all of the autophagy-defective pSTING mutants triggered cell apoptosis, which was associated with and participated in the antiviral functions. Additionally, pSTING lost its antiviral activity in TANK-binding kinase 1 $(TBK1)^{-/-}$ and IFN regulatory factor 3 $(IRF3)^{-/-}$ porcine macrophages, indicating the involvement of TBK1 and IRF3 in other STING activities such as apoptosis. Collectively, our results revealed that STING exerts both IFN- and autophagy-independent antiviral activity, and they also suggested that STING-triggered cell apoptosis resists viral infections.

IMPORTANCE The IFN-independent antiviral function of the cGAS-STING pathway has attracted great attention in recent years; however, the nature of this IFN-independent antiviral function is unknown, although STING-induced autophagy has been shown to mediate the STING antiviral activity. First, we analyzed the antiviral activity through the porcine cGAS-pSTING pathway and established that pSTING signaling exerts an IFN-independent antiviral function. Second, we found that pSTING-induced IFN-independent autophagy and the antiviral activity of pSTING are independent of both IFN and autophagy. Finally, pSTING signaling activates cell apoptosis independently of IFN and autophagy, and the apoptosis is associated with antiviral activity. Our results suggest that pSTING-activated apoptosis at least partially mediates the antiviral activity or multiple pSTING-activated signals, including IFN production, nuclear factor κ light chain enhancer of activated B cells (NF-κB) expression, autophagy, and apoptosis, exert a

Editor Bryan R. G. Williams, Hudson Institute of Medical Research

Copyright © 2022 American Society for Microbiology. All Rights Reserved.

Address correspondence to Jianzhong Zhu, jzzhu@yzu.edu.cn.

The authors declare no conflict of interest.

Received 27 September 2022
Accepted 27 October 2022
Published 15 November 2022

Downloaded from https://journals.asm.org/journal/jvi on 12 April 2023 by 147.100.179.233.

redundant antiviral role. Thus, the work reveals a new layer of complexity in STING antiviral activity.

KEYWORDS cGAS, STING, porcine, interferon, autophagy, apoptosis, antiviral

Innate immunity is the first line of defense against pathogenic microorganisms, recognizing the pathogen-associated molecular patterns (PAMPs) and damage-associated molecular patterns (DAMPs) (1, 2). The innate immune pattern recognition receptors (PRRs) are responsible for recognition of PAMPs and DAMPs, encompassing membrane-bound Toll-like receptors (TLRs) and C-type lectin-like receptors (CLRs) and cytosolic retinoic acid-inducible gene I (RIG-I)-like receptors (RLRs), nucleotide-binding oligomerization domain (NOD)-like receptors (NLRs), and cytosolic DNA receptors (CDRs). Upon activation by PAMPs or DAMPs, PRRs trigger transcription-dependent or -independent cell events and subsequently drive the expression of type I interferons (IFNs) or proinflammatory cytokines or protease activation, orchestrating innate immune responses (2).

Innate immune DNA receptors include TLR9 and CDRs (3). Among an array of CDRs, cyclic GMP-AMP synthase (cGAS) has been the most well defined and important DNA receptor (4). It belongs to the nucleotidyltransferase (NTase) family and can catalyze the substrates ATP and GTP into endogenous cyclic GMP-AMP (2′,3′-cGAMP), which, as a second messenger, activates the downstream endoplasmic reticulum (ER)-associated adaptor stimulator of IFN gene (STING) (5–8). Activated STING traffics to the ER-Golgi intermediate compartment (ERGIC) and Golgi, where it recruits TANK-binding kinase 1 (TBK1) through the (D/E)xPxPLR(S/T)D motif in its C-terminal tail (CTT). The recruited TBK1 is self-transactivated and phosphorylates conserved serine located in the IFN regulatory factor 3 (IRF3) recruitment motif (pLxIS) in the STING CTT (9). Next, the phosphorylated serine serves as a docking site to recruit the transcription factor IRF3, which is then phosphorylated by nearby TBK1 (10). The phosphorylated IRF3 forms a dimer and translocates into the nucleus to drive the expression of type I IFNs and the numerous IFN-stimulated genes (ISGs), inducing a robust antiviral state (11–13). In addition, STING activates nuclear factor κ light chain enhancer of activated B cells (NF-κB) to a small extent via the IKK$\alpha/\beta/\gamma$ complex, which is able to synergize with IRF3 in IFN production or drive proinflammatory cytokine production (14).

Beyond the IRF3- and NF-κB-mediated signaling, both cGAS and STING are able to activate autophagy, including canonical and noncanonical autophagy (15). STING-triggered autophagy was shown to exert an antiviral role independently of IFNs (16, 17). It was observed that STING is able to mediate ER stress and the unfolded protein response (UPR) through a novel and distinct motif named the UPR motif in the cyclic-dinucleotide-binding (CBD) domain, which negatively regulates the Akt/tuberous sclerosis complex (TSC)/mammalian target of rapamycin (mTOR) pathway to enhance canonical autophagy (18, 19). On the other hand, several studies revealed the detailed mechanisms of STING-triggered noncanonical autophagy (16, 20–22). Activated STING exits from the ER to the ERGIC and Golgi in a process dependent on the coat protein II (COP II) complex and Arf GTPases, and the ERGIC can serve as a membrane source for light chain 3 (LC3) lipidation and autophagosome biogenesis. Different from canonical autophagy, STING-triggered noncanonical autophagy is independent of upstream autophagy regulators such as ULK1, Beclin-1, and Atg9a but dependent on downstream autophagy regulators such as Atg5 and Atg16L1 (16). STING-induced noncanonical autophagy is mainly initiated by the direct interaction of STING with LC3 through the LC3-interacting regions (LIRs) on STING (21).

Recently, the IFN-independent antiviral activity of the cGAS-STING pathway has attracted attention from researchers (23), and STING-induced autophagy may be a contributor to such antiviral activity (16, 24–26). However, the antiviral activity of STING-induced autophagy has not been fully elucidated. In this study, we investigated porcine STING (pSTING) signaling against several viruses and found that pSTING exerts both IFN- and autophagy-independent antiviral activity. Furthermore, we found that STING-triggered cell apoptosis is involved in resistance to viral infections.

Downloaded from https://journals.asm.org/journal/jvi on 12 April 2023 by 147.100.179.233.

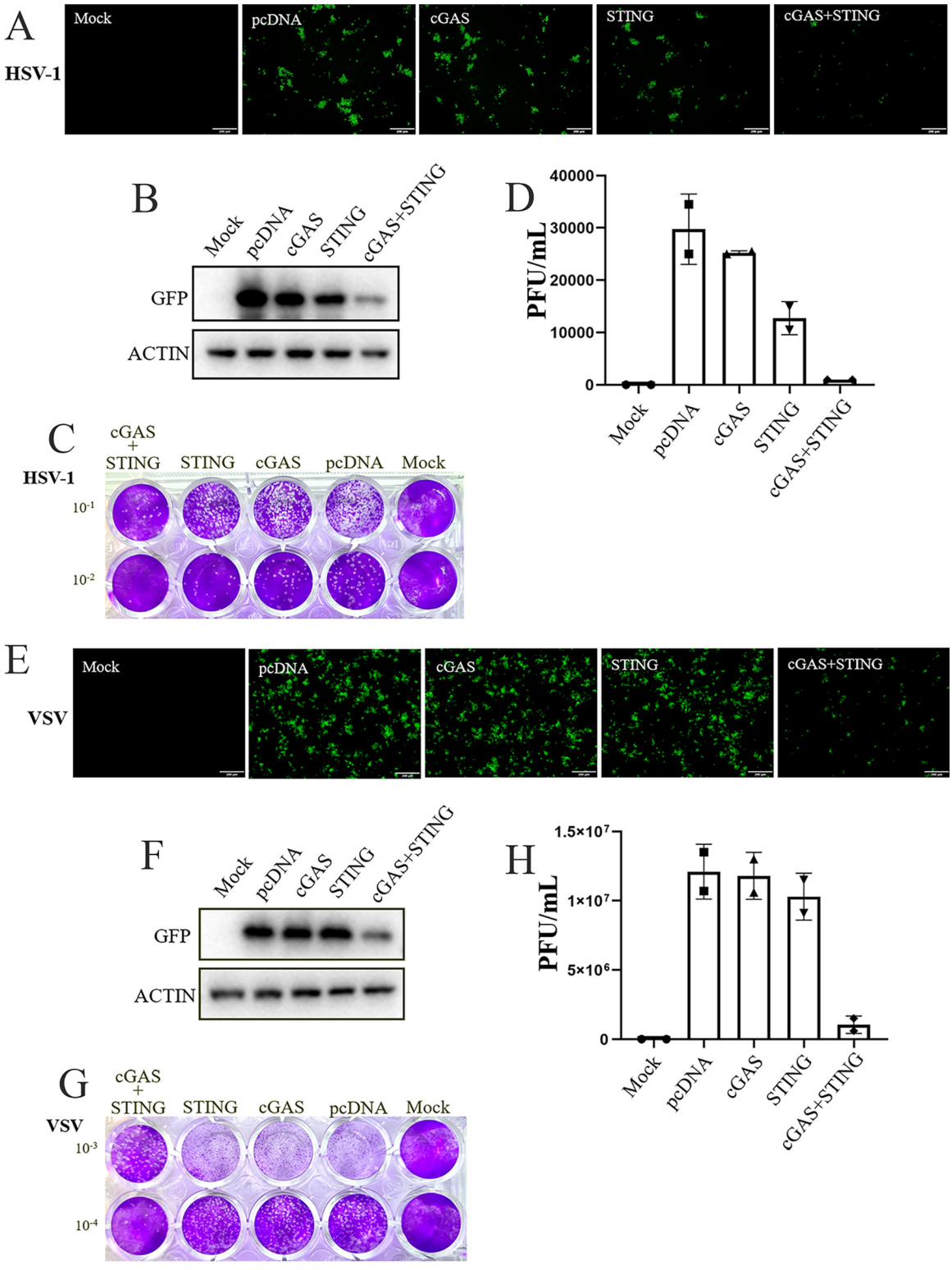

FIG 1 pcGAS-pSTING signaling restricts HSV-1 and VSV infections. (A to D) 293T cells in a 24-well plate (1.5×10^5 cells/well) were transfected with pcGAS (0.25 μg), pSTING (0.25 μg), pcGAS plus pSTING (0.25 μg plus 0.25 μg), or pcDNA control for 24 h. The transfected cells were infected with HSV-1-GFP (multiplicity of infection [MOI], 0.1) for another 24 h. The viral GFP fluorescence was observed by microscopy (A). The expression of viral GFP was detected by Western blotting (B). HSV-1 plaques are shown (C), and the numbers of plaques were counted (D). (E to H) 293T cells in a 24-well plate (1.5×10^5 cells/well) were transfected as in HSV-1 infection. The transfected cells were infected with VSV-GFP (MOI, 0.01) for another 12 h. The viral GFP fluorescence was observed by microscopy (E). The expression of viral GFP was detected by Western blotting (F). VSV plaques are shown (G), and the numbers of plaques were counted (H). The results in panels A to D and panels E to H are representative of three similar and independent experiments; the data in panels D and H are presented as the mean ± standard deviation (SD).

Downloaded from https://journals.asm.org/journal/jvi on 12 April 2023 by 147.100.179.233.

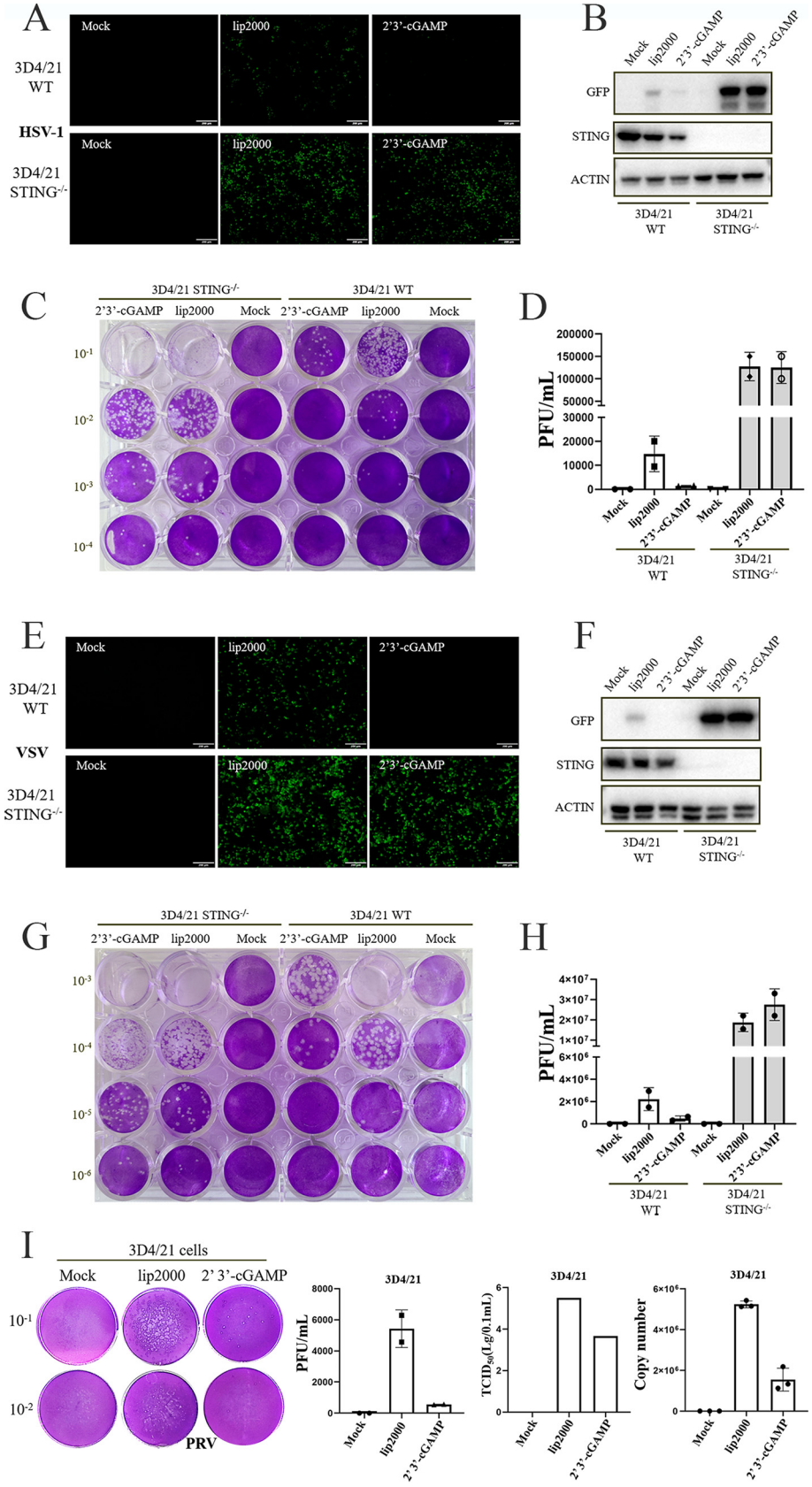

FIG 2 pSTING plays a key role in resisting HSV-1, VSV, and PRV. (A to D) STING$^{-/-}$ 3D4/21 and WT 3D4/21 cells grown in 24-well plates (1.5 $\times$ 10^5 cells/well) were stimulated with transfection of 2′,3′-cGAMP

(Continued on next page)

Downloaded from https://journals.asm.org/journal/jvi on 12 April 2023 by 147.100.179.233.

RESULTS

pSTING plays a critical role in resisting viral infections. To determine the antiviral effect of the porcine cGAS (pcGAS)-pSTING pathway, we transfected pcGAS and/or pSTING into 293T cells, followed by infection with herpes simplex virus 1 (HSV-1) or VSV. In HSV-1-infected cells, the results showed that pcGAS transfection alone could not induce anti-HSV-1 effects, while pSTING transfection alone had weak anti-HSV-1 effects. pSTING exhibited more pronounced anti-HSV-1 effects upon cotransfection and activation of pcGAS, as evidenced by green fluorescent protein (GFP) fluorescence microscopy, viral GFP Western blotting, and a viral plaque assay (Fig. 1A to D). With VSV infection, it could be observed that pSTING activated by pcGAS could induce anti-VSV effects (Fig. 1E to H).

To verify whether pSTING plays an essential role against viral infections, we utilized STING$^{-/-}$ 3D4/21 cells together with normal control 3D4/21 cells stimulated with the STING-specific agonist 2′,3′-cGAMP for infections with HSV-1 or VSV. The results showed that, in normal 3D4/21 cells, 2′,3′-cGAMP-stimulated pSTING signaling exhibited clear anti-HSV-1 effects, relative to the transfection control; in STING$^{-/-}$ 3D4/21 cells, HSV-1 replication was upregulated and 2′,3′-cGAMP lost its anti-HSV-1 effect (Fig. 2A to D). Similar results were noted with VSV infection (Fig. 2E to H). The 2′,3′-cGAMP-stimulated pSTING signaling also greatly inhibited the replication of porcine pseudorabies virus (PRV) (a DNA virus) in 3D4/21 cells, as evidenced by the plaque assay, 50% tissue culture infective dose ($TCID_{50}$) assay, and quantitative PCR (qPCR) assay (Fig. 2I). In STING$^{-/-}$ 3D4/21 cells, PRV replication was not upregulated; instead, PRV was downregulated, relative to the level in normal 3D4/21 cells. This is puzzling but interesting and needs to be further explored (see Fig. S1 in the supplemental material). Nevertheless, the 2′,3′-cGAMP lost its anti-PRV effect in STING$^{-/-}$ 3D4/21 cells (see Fig. S1). Taken together, the results suggested that pSTING signaling plays a key role in antiviral responses.

pSTING exerts an antiviral function independently of IFN. pSTING pLxIS sub is a mutant that has the IRF3 recruitment motif substituted with the chicken IRF7 recruitment motif and no longer induces IFN in mammalian cells, including 293T cells (27). We examined the antiviral function of pSTING pLxIS sub in transfected 293T cells. The results showed that the IFN-defective pSTING mutant exhibited more pronounced anti-HSV-1 and anti-Sendai virus (SeV) effects, compared with wild-type (WT) pSTING (Fig. 3A to C and G to I; also see Fig. S2A and C), and comparable anti-VSV effects, relative to WT pSTING (Fig. 3D to F; also see Fig. S2B), indicating the IFN-independent antiviral function of pSTING.

In order to further validate the IFN-independent antiviral function of pSTING, we constructed two additional pSTING mutants, namely, S365A and △CTT. The serine 365 of pSTING is the TBK1 phosphorylation site, and the phosphorylated serine 365 is for IRF3 recruitment and downstream IFN induction. The pSTING CTT contains both a TBK1 recruitment motif and a IRF3 recruitment motif and thus is essential for IFN induction. As expected, both pSTING mutants S365A and △CTT lost IFN activity in the IFN-stimulated response element (ISRE) promoter assay (Fig. 4A). Nevertheless, both mutants kept NF-κB activity, with S365A even showing higher NF-κB activity levels

FIG 2 Legend (Continued)
(2 μg/mL) by using Lipofectamine 2000. At 12 h posttransfection, the stimulated cells were infected with HSV-1-GFP (MOI, 0.1) for 24 h. The viral GFP fluorescence was observed by microscopy (A), and GFP expression was detected by Western blotting (B). The viral plaques are shown (C), and the numbers of plaques were plotted (D). (E to H) STING$^{-/-}$ 3D4/21 and WT 3D4/21 cells grown in 24-well plates (1.5×10^5 cells/well) were stimulated as in HSV-1 infection. At 12 h posttransfection, the stimulated cells were infected with VSV-GFP (MOI, 0.01) for 12 h. The viral GFP fluorescence was observed by microscopy (E), and GFP expression was detected by Western blotting (F). The viral plaques are shown (G), and the numbers of plaques were plotted (H). (I) 3D4/21 cells grown in a 24-well plate were stimulated with transfection of 2′,3′-cGAMP (2 μg/mL). At 12 h posttransfection, the stimulated cells were infected with PRV (MOI, 0.1) for 24 h. The viral titers were measured by plaque and $TCID_{50}$ assays, and viral genome copy numbers were determined by qPCR. The results in panels A to D, panels E to H, and panel I are representative of three, three, and two similar experiments, respectively; the data in the bar graphs are presented as mean ± SD.

Downloaded from https://journals.asm.org/journal/jvi on 12 April 2023 by 147.100.179.233.

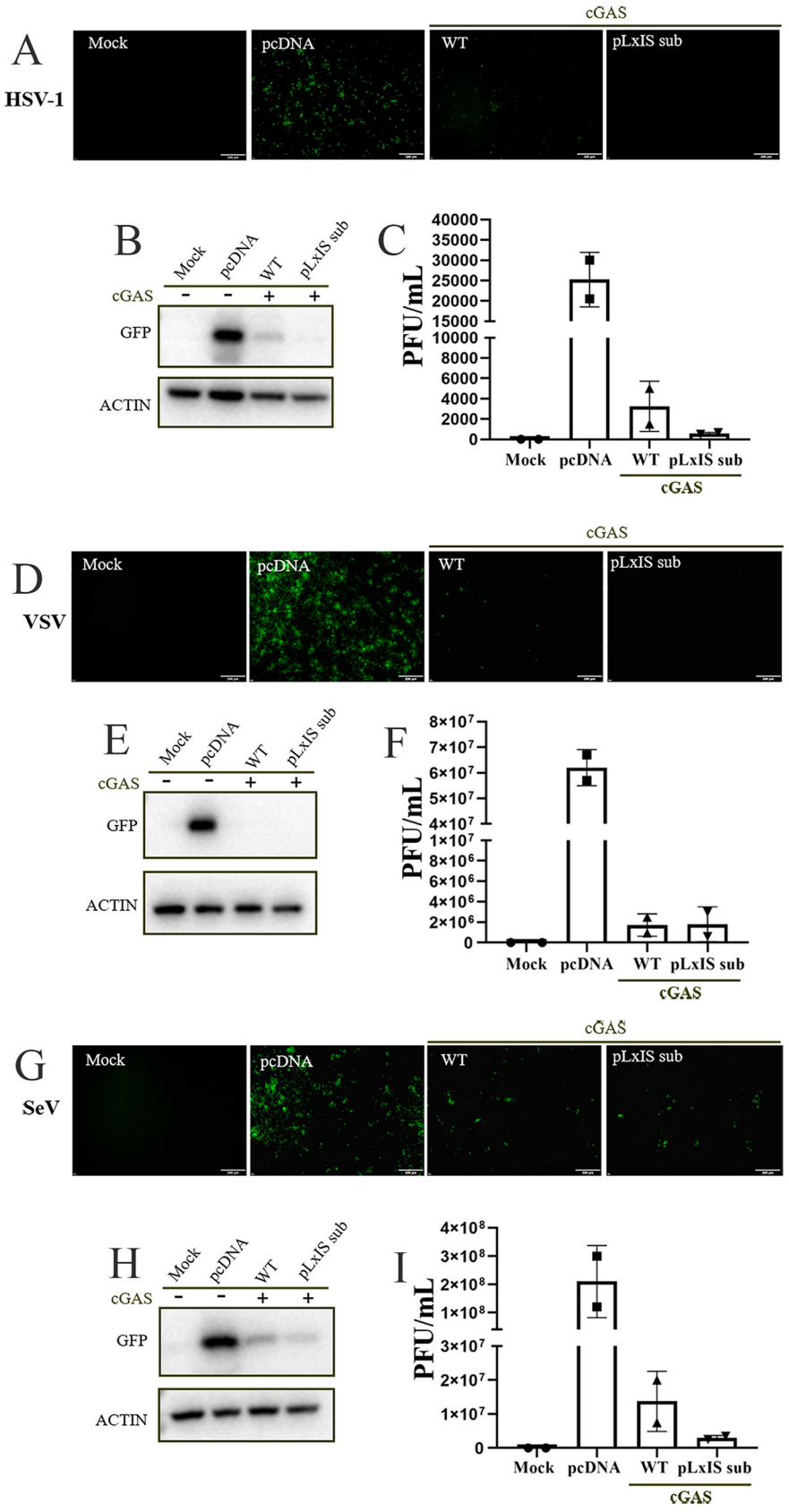

FIG 3 IFN-defective pSTING pLxIS sub exerts antiviral function. (A to C) 293T cells were transfected with cGAS (0.25 μg) combined with pSTING WT and pLxIS sub (0.25 μg each) for 24 h, with pcDNA

(Continued on next page)

Downloaded from https://journals.asm.org/journal/jvi on 12 April 2023 by 147.100.179.233.

than WT pSTING, indicating competition between IRF3 and NF-κB signals (Fig. 4B). Consistently, reverse transcription (RT)-qPCR assays showed that pSTING S365A and $\triangle$CTT could not induce IFN-β, ISG56, and ISG60 but could induce interleukin 8 (IL-8) and tumor necrosis factor alpha (TNF-α) (Fig. 4C). In Western blotting, pSTING S365A could induce TBK1 phosphorylation but not IRF3 phosphorylation and downstream ISG56 production, whereas pSTING $\triangle$CTT could not induce TBK1 and IRF3 phosphorylation and ISG56 production (Fig. 4D). The antiviral activities of pSTING S365A and $\triangle$CTT were examined in transfected 293T cells, and the results showed that both mutants S365A and $\triangle$CTT still possessed anti-HSV-1 activity (Fig. 4E to G; also see Fig. S2D) and anti-VSV activity (Fig. 4H to J; also see Fig. S2E), despite the defects in IFN activity. Taken together, these results clearly suggested that pSTING plays a strong antiviral role independently of IFN.

pSTING-induced autophagy does not depend on IFN but affects IFN. STING not only can induce IFN and inflammatory cytokines but also can induce autophagy (16, 20, 21). The autophagy induction by pSTING and three IFN-defective pSTING mutants was examined in transfected 293T cells, and the results showed that the three IFN-defective pSTING mutants, i.e., pLxIS sub, S365A, and $\triangle$CTT, all induced comparable lipid-bound LC3 (LC3-II) and phosphorylated p62 (p-p62) levels, relative to WT pSTING, suggesting that pSTING-induced autophagy was independent of IFN (Fig. 5A). Previously, a small region (residues 330 to 334) of human STING was identified as being important for autophagy induction, and point mutations of L333 and R334 within this region of STING abrogated LC3 lipidation (11). We made the equivalent point mutations in pSTING WT, S365A, and $\triangle$CTT and tested the autophagy induction by these L333A/R334A mutants in transfected 293T cells. Compared with WT pSTING, pSTING L333A/R334A had decreased levels of LC3-II (Fig. 5E, lane 12 versus lane 9). Similarly, for both pSTING S365A and pSTING $\triangle$CTT, the L333A/R334A mutation decreased the levels of LC3-II and p-p62 (Fig. 5B). Because L333A/R334A mutation also decreased the expression of various pSTING proteins (Fig. 5B and E), the pSTING WT, S365A, and $\triangle$CTT protein expression levels were titrated and adjusted for expression levels equal to those of the corresponding L333A/R334A mutants (Fig. 5C, D, and F). After avoiding the disturbance of pSTING expression, the L333A/R334A mutation was validated to dampen the autophagy by pSTING WT, S365A, and $\triangle$CTT (Fig. 5C, D, and F).

Human STING was shown to directly activate autophagy by interacting with LC3 through the LIRs, involving LIR4, LIR6, and LIR7 of the STING CBD (21). Based on the alignment of human STING and pSTING (Fig. S3), only LIR4 and LIR7 are present in pSTING, and point mutations of LIR4 (Y167A/L170A) and LIR7 (Y245A/L248A) were made separately in pSTING WT, S365A, and $\triangle$CTT (Fig. 5E). The pSTING mutants Y167A/L170A and Y245A/L248A were tested for autophagy induction in transfected 293T cells, and the results showed that either Y167A/L170A or Y245A/L248A mutations in various pSTINGs decreased the LC3-II levels to basal levels, as in the porcine cDNA (pcDNA)-transfected control (Fig. 5E). Again, after adjustment of the protein expression levels of pSTING WT, S365A, and $\triangle$CTT to be as low as those of the corresponding Y167A/L170A or Y245A/L248A mutants (Fig. 5F and G), the Y167A/L170A or Y245A/L248A mutation was validated to abrogate the autophagy by pSTING WT, S365A, and $\triangle$CTT (Fig. 5E to G).

FIG 3 Legend (Continued)
transfection and mock transfection as controls. The cells were next infected with HSV-1-GFP (MOI, 0.1) for another 24 h, followed by detection of viral replication with GFP fluorescence (A), GFP expression (B), and viral plaque assay (C). (D to I) 293T cells were transfected as in HSV-1 infection and infected with VSV-GFP (MOI, 0.01) (D to F) for 12 h or SeV-GFP (MOI, 0.01) (G to I) for 12 h. The viral replication was detected by GFP fluorescence transfection (D and G), GFP expression (E and H), and plaque assay (F and I). The results in panels A to C, panels D to F, and panels G to I are representative of three, three, and two similar experiments, respectively; the data in bar graphs are presented as mean $\pm$ SD.

Downloaded from https://journals.asm.org/journal/jvi on 12 April 2023 by 147.100.179.233.

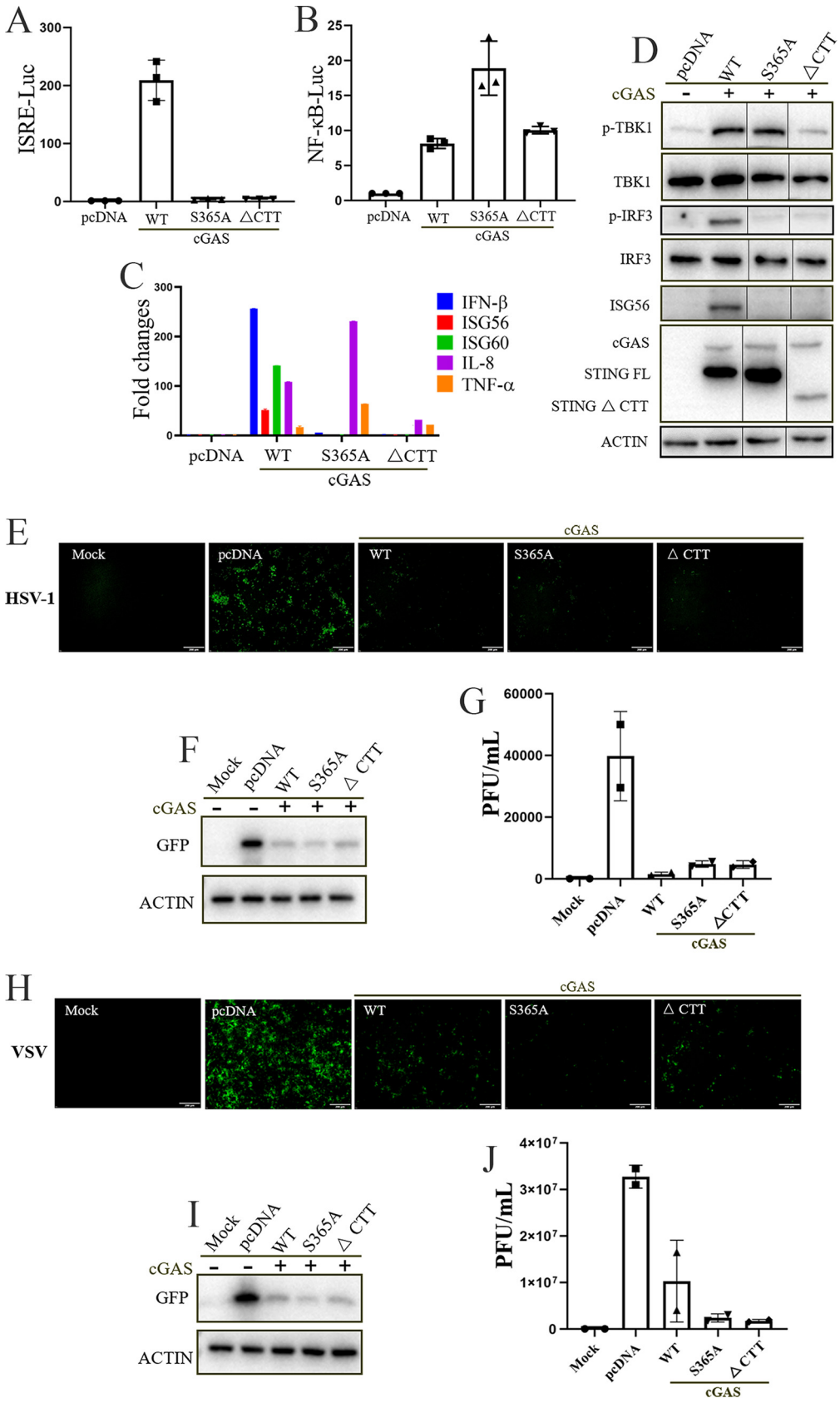

FIG 4 IFN-defective pSTING S365A and △CTT also exert antiviral function. (A and B) 293T cells in a 96-well plate (3×10^4 cells/well) were transfected with the indicated combinations of pcGAS (20 ng) and pSTING WT/S365A/

(Continued on next page)

Downloaded from https://journals.asm.org/journal/jvi on 12 April 2023 by 147.100.179.233.

The aforementioned pSTING autophagy mutants were further examined for IFN and NF-κB activity. L333A/R334A, Y167A/L170A, and Y245A/L248A mutations all decreased pSTING-induced levels of phosphorylated TBK1 (p-TBK1) and phosphorylated IRF3 (p-IRF3) (Fig. 5E, lanes 9 to 12), as well as ISRE promoter activity (Fig. 5H). On the other hand, all of these autophagy mutations also decreased the NF-κB promoter activity triggered by pSTING WT, S365A, and $\triangle$CTT (Fig. 5I). Taken together, the results described above suggest that pSTING triggers IFN-independent autophagy, despite the fact that pSTING-activated autophagy influences STING-downstream IFN and NF-κB activity.

pSTING enables resistance to viral infections independently of both IFN and autophagy. Since it seems that the antiviral function of pSTING is associated with its autophagy activity, the various pSTING autophagy mutants in the context of pSTING WT, S365A, and $\triangle$CTT were tested for anti-HSV-1 and anti-VSV effects in transfected 293T cells. The antiviral effects were indicated by GFP microscopy (Fig. 6A and F), GFP Western blotting (Fig. 6B and G), and plaque assays (Fig. 6C to E and H to J). Surprisingly, the various Y167A/L170A and Y245A/L248A mutants of pSTING WT, S365A, and $\triangle$CTT, in which the mutation abrogated the autophagy activity, exhibited comparable anti-HSV-1 effects, relative to the corresponding pSTING WT, S365A, and $\triangle$CTT (Fig. 6A to E; also see Fig. S4A to C). On the contrary, the various L333A/R334A mutants of pSTING WT, S365A, and $\triangle$CTT, in which the mutation dampened the autophagy activity, exhibited strong anti-HSV-1 effects despite the decreased antiviral activity, relative to the corresponding pSTING WT, S365A, and $\triangle$CTT (Fig. 6A to E; also see Fig. S4A to C). Similar results were obtained in the VSV infection setting (Fig. 6F to J; also see Fig. S4D to F).

These results clearly suggest that pSTING exerts an antiviral function in a way that is not only independent of its IFN activity but also independent of its autophagy activity. It also further suggests that pSTING exerts an antiviral function in a way that is independent of both IFN and autophagy.

pSTING induces apoptosis independently of both IFN and autophagy. STING has been implicated as inducing cell apoptosis (28). Thus, we continued to explore whether pSTING can induce apoptosis after losing IFN and autophagy activities. To this end, pSTING WT, pLxIS sub, S365A, and $\triangle$CTT and all autophagy mutants in the context of pSTING WT, S365A, and $\triangle$CTT were transfected into 293T cells to detect their apoptotic activity (Fig. 7). Flow cytometry showed that all pSTING forms, including those that were defective in both IFN and autophagy, were able to induce apoptosis upon pcGAS stimulation, whereas pcGAS or pSTING alone was unable to induce apoptosis (Fig. 7A to C; also see Fig. S5A to C). Among various pSTING mutants, the L333A/R334A mutants of pSTING WT, S365A, and $\triangle$CTT exhibited decreased apoptosis, relative to the corresponding pSTING WT, S365A, and $\triangle$CTT, but still kept the ability to induce both early and late cell apoptosis (Fig. 7B and C). Since pSTING induces apoptosis and antiviral effects, independently of both IFN and autophagy, this indicates that pSTING-induced apoptosis and antiviral activity are associated with each other. Furthermore, the induction of apoptosis may be involved in the pSTING antiviral function. Indeed, when

FIG 4 Legend (Continued)
$\triangle$CTT (20 ng each), or empty vector (40 ng), together with ISRE Fluc (10 ng) (A) or NF-κB Fluc (10 ng) (B) plus Rluc (0.2 ng). Luciferase activities were measured 24 h after transfection. (C) 293T cells grown in a 12-well plate (3×10^5 cells/well) were transfected with the indicated combinations of pcGAS (0.5 μg) and pSTING WT/S365A/$\triangle$CTT (0.5 μg each) for 48 h. The RNA expression of human IFN-β, human ISG56, human ISG60, human IL-8, and human TNF-α was analyzed by RT-qPCR. (D) 293T cells grown in a 24-well plate (1.5×10^5 cells/well) were transfected with the indicated combinations of pcGAS (0.25 μg) and pSTING WT/S365A/$\triangle$CTT (0.25 μg each) or empty pcDNA vector (0.5 μg) for 24 h, and the expression of p-TBK1, TBK1, p-IRF3, IRF3, ISG56, cGAS-HA, and STING-HA was examined by Western blotting. The protein bands separated by vertical lines were from noncontiguous portions of one gel. (E to J) 293T cells were transfected with pcGAS (0.25 μg) combined with pSTING WT/S365A/$\triangle$CTT (0.25 μg each) for 24 h, with pcDNA transfection and mock transfection as controls. The treated cells were infected with HSV-1-GFP (MOI, 0.1) (E to G) for 24 h or VSV-GFP (MOI, 0.01) (H to J) for 12 h, followed by detection of viral replication with GFP fluorescence (E and H), GFP expression (F and I), and plaque assay (G and J). The results in panels A to D, panels E to G, and panels H to J are representative of two, three and three similar experiments, respectively.

Downloaded from https://journals.asm.org/journal/jvi on 12 April 2023 by 147.100.179.233.

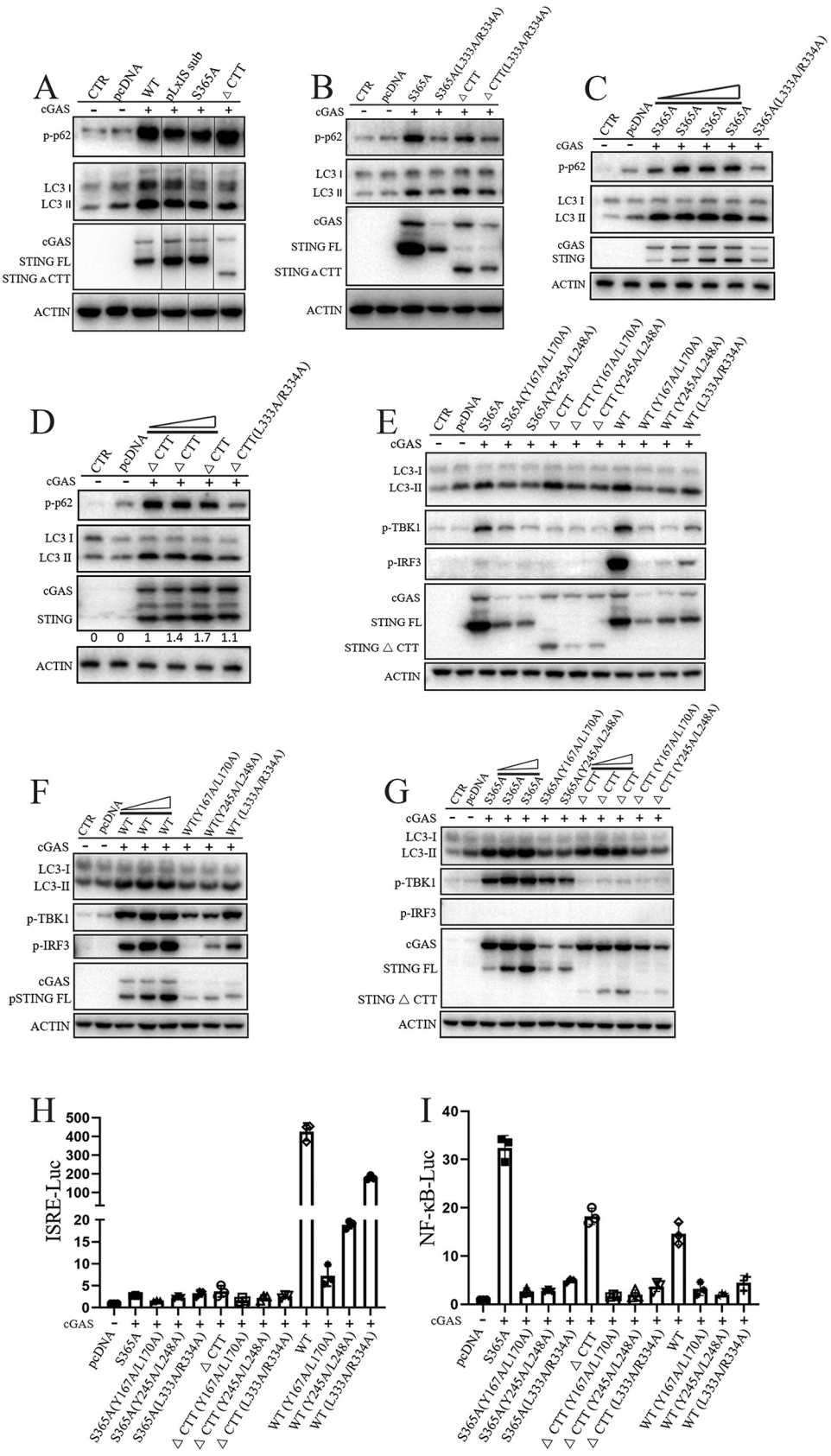

FIG 5 Analysis of autophagy, IFN, and NF-κB activities of various pSTING mutants. (A) 293T cells grown in a 24-well plate (1.5×10^5 cells/well) were transfected with the indicated combinations of pcGAS (0.25 μg) and

(Continued on next page)

Downloaded from https://journals.asm.org/journal/jvi on 12 April 2023 by 147.100.179.233.

3D4/21 cells were treated with two caspase inhibitors, i.e., *N*-acetyl-Asp-Glu-Val-Asp-aldehyde (Ac-DEVD-CHO) and carbobenzoxy-Val-Ala-Asp-(*O*-methyl)-fluoromethyl ketone (Z-VAD-FMK), to inhibit cell apoptosis, the antiviral activity of 2′,3′-cGAMP-stimulated STING signaling was obviously reversed in an inhibitor dose-dependent manner (Fig. 7D to G). Thus, the results suggest that pSTING-induced apoptosis participates in the antiviral effect at least in part.

Both TBK1 and IRF3 are necessary for pSTING to exert antiviral function. Next, we explored the roles of downstream TBK1 and IRF3 in the antiviral functions of pSTING. To this end, TBK1 and IRF3 were knocked out from porcine macrophages 3D4/21 through the CRISPR-Cas9 approach (Fig. 8). In TBK1$^{-/-}$ 3D4/21 cells, both HSV-1 and VSV replication was greatly upregulated and 2′,3′-cGAMP activation of pSTING lost the anti-HSV-1 (Fig. 8A to C) and anti-VSV (Fig. 8D to F) effects, relative to normal 3D4/21 cells, as evidenced by GFP microscopy, GFP Western blotting, and plaque assays (Fig. 8A to F; also see Fig. S6A and B). In IRF3$^{-/-}$ 3D4/21 cells, the same viral infection results were obtained, i.e., both HSV-1 and VSV replication was greatly upregulated and 2′,3′-cGAMP lost the antiviral function (Fig. 8G to L; also see Fig. S6C and D). These results suggest that, although the antiviral function of pSTING is independent of the activation of the TBK1-IRF3 signal axis and subsequent downstream production of IFN, the presence of both TBK1 and IRF3 is required.

DISCUSSION

The cGAS-STING pathway-mediated IFN signaling plays a key role against viral infections (13). It has been appreciated that the cGAS-STING-mediated IFN-independent signal events also play an important role in restricting HSV-1 infection (17, 29, 30); nevertheless, the nature of the IFN-independent antiviral activity of STING remains unclear (23). Our study first confirmed the IFN-independent antiviral activity of pSTING (Fig. 3 and 4) and next explored the nature of such IFN-independent antiviral activity. In addition to IFN production, STING signaling at least activates autophagy, NF-κB, and cell death (23, 31). First, despite several studies suggesting that STING-induced autophagy mediates antiviral function (16, 24–26), our study clearly demonstrated that STING-induced autophagy is dispensable for either anti-HSV-1 or anti-VSV activity. Second, two other studies suggested that NF-κB is implicated in STING antiviral activity (30, 32). In our study, the autophagy-defective pSTING mutants also showed a substantial reduction of NF-κB activity (Fig. 5I), but the antiviral activities of these pSTING mutants were not altered (Fig. 6), indicating that NF-κB is also dispensable for STING antiviral activity. Finally, we found that pSTING can induce cell apoptosis independently of IFN and autophagy and the induced apoptosis is clearly associated with and participates in the antiviral activity (Fig. 7). Therefore, our study revealed the additional machinery utilized by STING to restrict and resist viral infections.

In this study, we confirmed that pSTING induces IFN-independent autophagy, and both LIR4/LIR7 and L333/R334 located in the CBD of pSTING are essential for autoph-

FIG 5 Legend (Continued)
pSTING WT/pLxIS sub/S365A/△CTT (0.25 μg each) for 24 h, and the indicated protein expression was analyzed by Western blotting. The protein bands separated by vertical lines were from noncontiguous portions of one gel. (B) 293T cells were transfected with the indicated combinations of pcGAS (0.25 μg) plus pSTING S365A or △CTT and the corresponding L333A/R334A mutants (0.25 μg each) for 24 h, followed by Western blotting. (C and D) 293T cells were transfected with the indicated combinations of pcGAS (0.25 μg) plus a S365A gradient (0.1, 0.15, 0.2, and 0.25 μg) and S365A L333A/R334A (0.25 μg) (C) or a △CTT gradient (0.05, 0.15, and 0.25 μg) and △CTT L333A/R334A (0.25 μg) (D) for 24 h. (E) 293T cells were transfected with pcGAS (0.25 μg) combined with pSTING WT, S365A, or △CTT or various Y167A/L170A, Y245A/L248A, or L333A/R334A mutants (0.25 μg each), as indicated, for 24 h. (F) 293T cells were transfected with pcGAS (0.25 μg) combined with a pSTING WT gradient (0.05, 0.15, and 0.25 μg) and the mutants Y167A/L170A, Y245A/L248A, and L333A/R334A (0.25 μg each) for 24 h. (G) 293T cells were transfected with pcGAS (0.25 μg) combined with a pSTING S365 gradient (0.05, 0.15, and 0.25 μg) or a △CTT gradient (0.05, 0.15, and 0.25 μg) and the corresponding mutants Y167A/L170A and Y245A/L248A (0.25 μg each) for 24 h. (H and I) 293T cells in a 96-well plate were transfected with pcGAS (20 ng) combined with pSTING WT, S365A, or △CTT or various mutants, as indicated (20 ng each), plus ISRE FLuc and Rluc (H) or plus ELAM (NF-κB) Fluc and Rluc (I). Luciferase activities were measured 24 h posttransfection. All results are representative of two similar experiments.

Downloaded from https://journals.asm.org/journal/jvi on 12 April 2023 by 147.100.179.233.

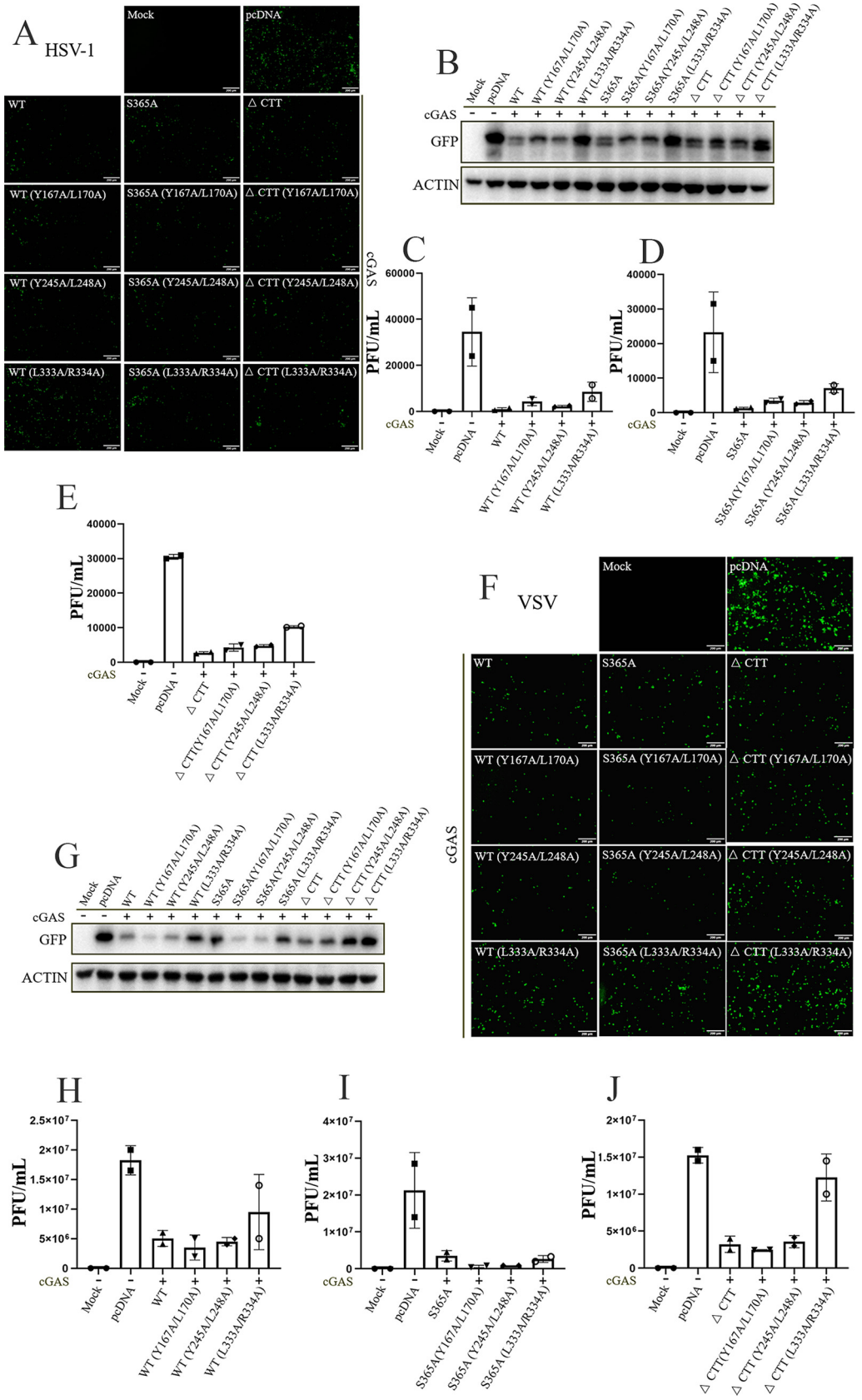

FIG 6 pSTING can resist viruses independently of both IFN and autophagy activity. (A to E) 293T cells were transfected with pcGAS (0.25 μg) combined with pSTING WT, S365A, or △CTT, various mutants, or the pcDNA control as indicated

(Continued on next page)

Downloaded from https://journals.asm.org/journal/jvi on 12 April 2023 by 147.100.179.233.

agy induction. Among these sites, LIR4 and LIR7 are unquestionably involved in STING-induced noncanonical autophagy by mediating the interaction of STING and LC3 (21). Although the residues L333 and R334 and the corresponding small region (residues 330 to 334) of human STING were identified as being important for autophagy, the machinery of these STING sites inducing noncanonical autophagy is unknown (16). We noticed that this small region is located within the STING UPR motif (residues 322 to 343), which was initially identified as being responsible for STING-activated ER stress and subsequent T cell death (19). The STING-induced ER stress likely leads to canonical autophagy with mTOR inactivation involved (18). Therefore, LIR4/LIR7 and L333/R334 seem to participate in the induction of autophagy with distinct mechanisms; nevertheless, both sites are implicated in the IFN and NF-κB signals of pSTING (Fig. 5H and I), and neither is required for the antiviral function of pSTING (Fig. 6).

STING weakly induces NF-κB signaling relative to IRF3 signaling, but the exact mechanism remains unresolved (31). On one hand, TBK1 was shown to be required for or to participate redundantly with IKKε in the STING-induced NF-κB activation (14, 33, 34). On the other hand, STING kept the ability to activate NF-κB without the CTT domain, which excluded the participation and requirement of TBK1 (35, 36). Our results showed that pSTING $\triangle$CTT is able to induce comparable NF-κB expression (Fig. 4B and 5I), suggesting that CTT and TBK1 are not necessary for STING-activated NF-κB signaling, which is similar to the case for autophagy. Additionally, pSTING-induced NF-κB activity was positively regulated by autophagy (Fig. 5I), indicating that the two may be intrinsically linked. The results are supported by invertebrate STINGs that lack the CTT but enable NF-κB and autophagy activation and antiviral functions (16, 37). It is possible that STING may activate NF-κB alternatively, depending on the signal in the CBD of oligomerized STING (31). In terms of the antiviral function, our results indicate that NF-κB is also not necessary for STING antiviral activity.

STING contributes to different types of cell death, such as apoptosis, lysosomal cell death (LCD), pyroptosis, and necroptosis (31, 38). Our study found that pSTING can induce cell apoptosis independently of its IFN and autophagy activities and further that the induced apoptosis is well associated with and participates in the antiviral activity (Fig. 6 and 7). These results suggest that STING-activated apoptosis exerts antiviral functions even though it has been shown to induce B cell/T cell death and immune evasion (19, 28) but never direct and clear antiviral functions. Thus, we found here one additional antiviral mechanism of pSTING signaling. STING was shown to induce cell apoptosis via its UPR motif activating ER stress or via downstream IRF3 binding with Bax (38). Our study also showed that the presence of both TBK1 and IRF3 is required for STING-induced antiviral activity (Fig. 8). The results suggest that both TBK1 and IRF3 might participate in STING-induced cell apoptosis and antiviral function but in a way independent of IFN.

Our findings regarding the pSTING antiviral machinery were mainly based on transfected 293T cells, which have been widely and commonly used for studies on cGAS-STING signaling due to their lack of endogenous cGAS and STING expressions (4, 39). Therefore, the observations and conclusions are biologically relevant and significant. Nevertheless, the findings need to be validated in STING$^{-/-}$ macrophages through reconstitutions of various pSTING mutants and subsequent antiviral experiments. We considered and tried the reconstitution experiments using plasmid transfections; unfortunately, the reconstituted pSTING signaling is weak and fails to exert antiviral effects. Reconstitutions using either lentivirus or retrovirus transduction should

FIG 6 Legend (Continued)
(0.25 μg each) for 24 h. The transfected cells were infected with HSV-1-GFP (MOI, 0.1) for another 24 h, followed by detection of viral replication with GFP fluorescence (A), GFP expression (B), and plaque assay (C to E). (F to J) 293T cells were transfected as in HSV-1 infection, and the transfected cells were infected with VSV-GFP (MOI, 0.01) for 12 h, followed by detection of viral replication with GFP fluorescence (F), GFP expression (G), and plaque assay (H to J). All results are representative of three similar experiments.

Downloaded from https://journals.asm.org/journal/jvi on 12 April 2023 by 147.100.179.233.

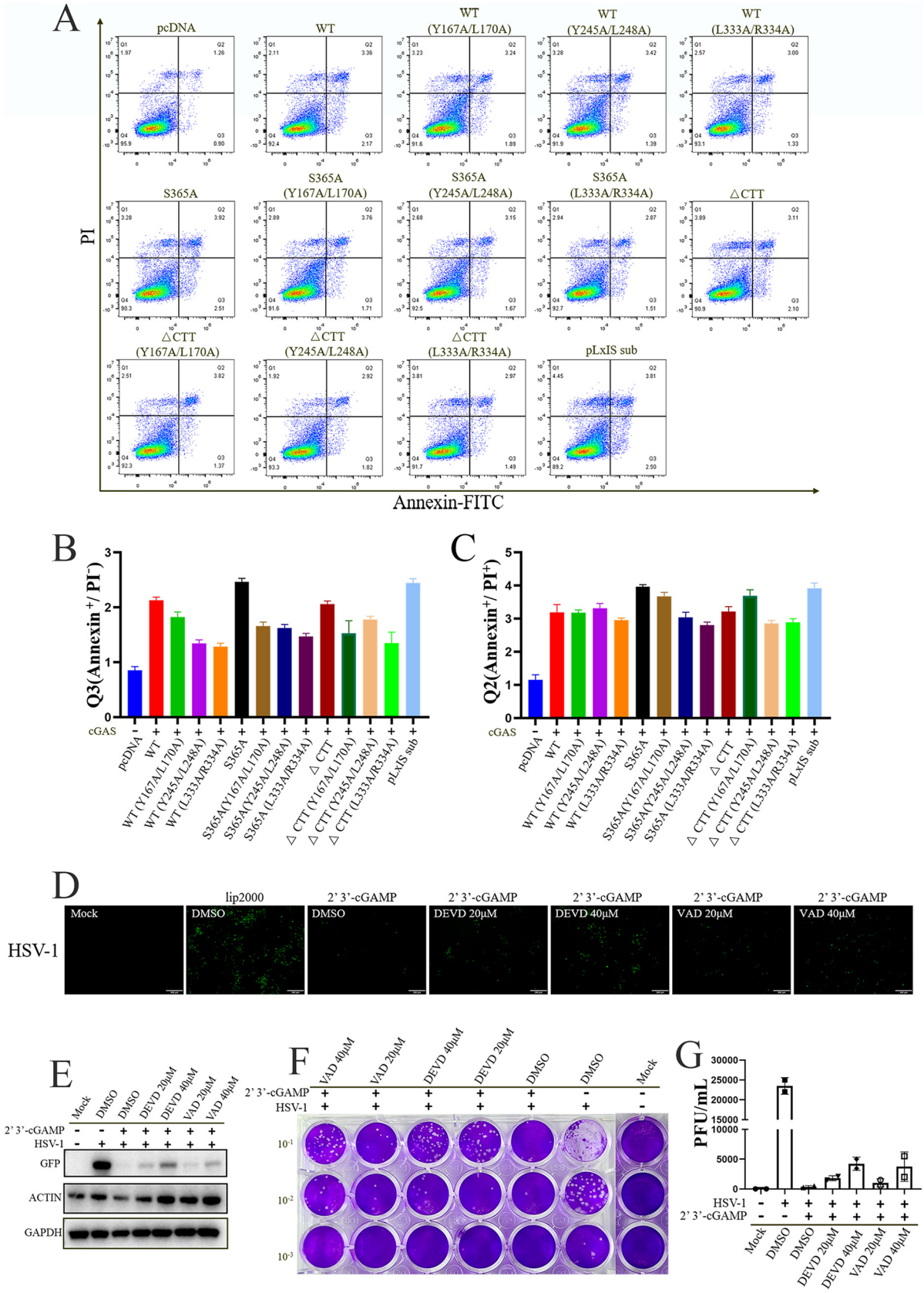

FIG 7 pSTING-induced apoptosis mediates antiviral function independently of both IFN and autophagy activity. (A to C) 293T cells were transfected with pcGAS (0.25 μg) combined with pSTING WT, S365A, or △CTT, various mutants, or pLxIS sub, as indicated (0.25 μg each),

(Continued on next page)

Downloaded from https://journals.asm.org/journal/jvi on 12 April 2023 by 147.100.179.233.

improve the process, likely giving the desired results, and thus deserve further investigation.

Multiple studies, including ours, have shown that cGAS-STING signaling exhibits broad-spectrum antiviral functions, including anti-RNA virus functions (40, 41). The principle underlying the mechanism of cGAS-STING-mediated activity against RNA viruses is the sensing of damaged mitochondrial and genomic DNA leaked into the cytoplasm during infections and the subsequent activation of STING-downstream events such as IFN production, autophagy, and/or cell apoptosis (41). Interestingly, one such study found that STING-dependent translation inhibition, independent of the RNA signaling adaptor mitochondrial antiviral signaling protein (MAVS), IFN, and autophagy, prevents RNA virus infection (42). Thus, this adds a layer of complexity to the STING antiviral machinery while broadening our vision.

In summary, our study reveals that pSTING exerts an intriguing antiviral function independent of both IFN and autophagy (see Fig. S7 in the supplemental material). The STING antiviral function is partly mediated by cell apoptosis or by several STING signaling events, including IFN expression, NF-κB activation, autophagy, apoptosis, and/or others, likely in a redundant manner. Considering the conservation of the cGAS-STING pathway along evolution, our findings provide deep insights into the STING immune biology in viral infections.

MATERIALS AND METHODS

Reagents and antibodies. TRIpure reagent was purchased from Aidlab (Beijing, China). The annexin V-fluorescein isothiocyanate (FITC)/propidium iodide (PI) apoptosis detection kit, HiScript first-strand cDNA synthesis kit, ChamQ universal SYBR qPCR master mix, 2×*Taq* Master Mix (Dye Plus), and 180-kDa prestained protein markers were all from Vazyme Biotech Co., Ltd. (Nanjing, China). The Golden Star T6 Super PCR mix polymerase was from by Tsingke (Nanjing, China). The double-luciferase reporter assay kit was purchased from TransGen Biotech (Beijing, China). 2′,3′-cGAMP was purchased from InvivoGen (Hong Kong, China). Low-melting-point agarose was purchased from Sigma-Aldrich (St. Louis, MO, USA). HSV-1-GFP (KOS strain) (40), VSV-GFP (Indiana HR strain) (40, 43), SeV-GFP (40), and porcine PRV (Bartha K61 strain [GenBank accession number JF797217]) were preserved in our laboratory. Apoptosis inhibitors Ac-DEVD-CHO (a caspase 3 inhibitor) and Z-VAD-FMK (a pan-caspase inhibitor) were from Beyotime Biotechnology (Shanghai, China). All other chemicals and reagents were analytical grade and obtained commercially.

The mouse anti-actin monoclonal antibody (MAb) and mouse anti-GFP MAb were acquired from TransGen Biotech. The rabbit STING polyclonal antibody (PAb) (19851-1-AP) and rabbit p-p62 PAb (18420-1-AP) were both purchased from ProteinTech (Wuhan, China). The mouse glyceraldehyde 3-phosphate dehydrogenase (GAPDH) MAb was from ABclonal (Wuhan, China). The rabbit TBK1 MAb (3504S), rabbit p-TBK1 (Ser172) MAb (5483S), IRF3 MAb (11904S), hemagglutinin (HA) MAb (3724), and rabbit LC3B (D11) XP MAb (3868) were all acquired from Cell Signaling Technology (Boston, MA, USA). The rabbit p-IRF3 (Ser385) PAb (MA5-14947) was purchased from Thermo Fisher Scientific (Sunnyvale, CA, USA). Rabbit ISG56 PAb was homemade and stored in our laboratory. Horseradish peroxidase (HRP)-conjugated goat anti-rabbit IgG (H+L) highly cross-adsorbed secondary antibody and goat anti-mouse IgG (H+L) highly cross-adsorbed secondary antibody were obtained from Sangon Biotech (Shanghai, China).

Cells and cell transfection. HEK-293T cells (ATCC catalog number CRL-3216), Vero cells (ATCC catalog number CCL-81), and PK15 cells (ATCC catalog number CCL-33) were maintained in Dulbecco's modified Eagle's medium (DMEM) (HyClone Laboratories, USA) supplemented with 10% fetal bovine serum (FBS) (Gibco, USA) and 1% penicillin-streptomycin and were maintained at 37°C with 5% CO_2. Porcine macrophage 3D4/21 cells (ATCC catalog number CRL-2843) were cultured in RPMI 1640 medium (HyClone Laboratories, USA) supplemented with 10% FBS and 1% penicillin-streptomycin and were maintained at 37°C with 5% CO_2. Transfection was performed by using Lipofectamine 2000 (Thermo Fisher Scientific) following the manufacturer's instructions.

Molecular cloning and gene mutations. The HA-tagged pcDNA DEST plasmids of pcGAS and pSTING were previously constructed and characterized (27, 44) and have been used in our laboratory. The PCR primers for pSTING mutations were designed using the QuikChange primer design method

FIG 7 Legend (Continued)
for 48 h. The apoptosis of transfected cells was analyzed using annexin V-FITC/PI staining followed by flow cytometry. The dot plots of cell apoptosis in various samples are presented (A). The early apoptosis as indicated by Q3 (annexin positive and PI negative) (B) and late apoptosis as indicated by Q2 (annexin positive and PI positive) (C) are plotted as bar graphs. (D to G) 3D4/21 cells grown in a 24-well plate were treated with two apoptosis inhibitors, i.e., Ac-DEVD-CHO and Z-VAD-FMK, at the indicated concentrations for 30 min, followed by stimulation with transfection of 2′,3′-cGAMP (2 μg/mL) for 12 h. The stimulated cells were infected with HSV-1-GFP (MOI, 0.1) for another 24 h, followed by detection of viral replication with GFP fluorescence (D), GFP expression (E), and plaque assay (F to G). DMSO, dimethyl sulfoxide. The results in panels A to C and panels D to G are representative of three and two similar experiments, respectively.

Downloaded from https://journals.asm.org/journal/jvi on 12 April 2023 by 147.100.179.233.

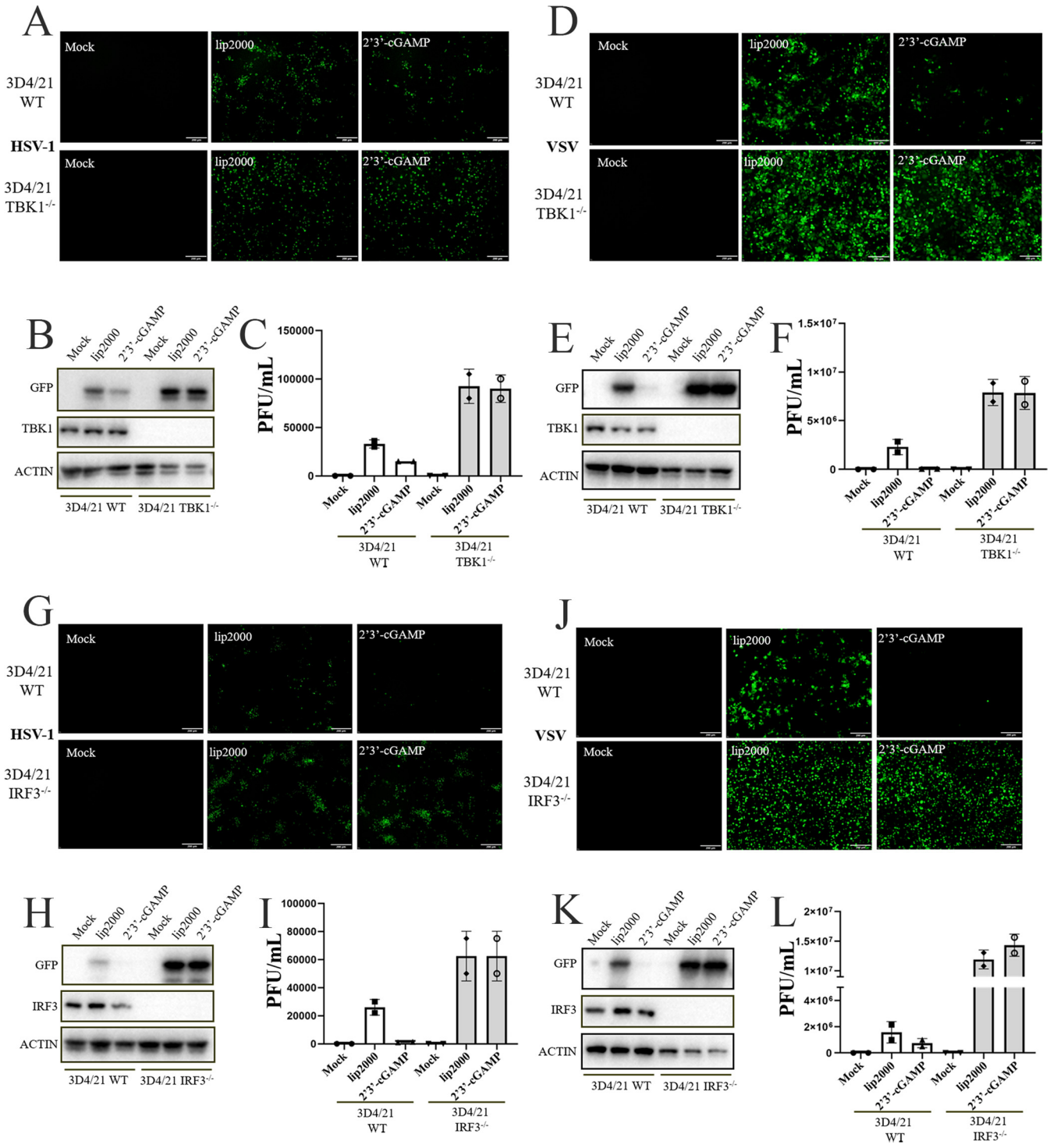

FIG 8 The presence of TBK1 and IRF3 is necessary for the antiviral function of pSTING. (A to F) TBK1$^{-/-}$ 3D4/21 and WT 3D4/21 cells in a 24-well plate were stimulated with transfection of 2′,3′-cGAMP (2 μg/mL) using Lipofectamine 2000 for 12 h. The stimulated cells were infected with HSV-1-GFP (MOI, 0.1) (A to C) for 24 h or VSV-GFP (MOI, 0.01) (D to F) for 12 h, followed by detection of viral replication with GFP fluorescence (A and D), GFP expression (B and E), and plaque assay (C and F). (G to K) IRF3$^{-/-}$ 3D4/21 and WT 3D4/21 cells in a 24-well plate were stimulated with transfection of 2′,3′-cGAMP (2 μg/mL) for 12 h. The stimulated cells were infected with HSV-1-GFP (MOI, 0.1) (G to I) for 24 h or VSV-GFP (MOI, 0.01) (J to L) for 12 h, followed by detection of viral replication with GFP fluorescence (G and J), GFP expression (H and K), and plaque assay (I and L). All results are representative of three similar experiments.

(Agilent) and are shown in Table S1 in the supplemental material. The mutation PCR was performed with KOD plus Neo polymerase (Toyobo, Shanghai, China) and pcDNA-pSTING-2HA as the template. The PCR products were transformed into competent DMT *Escherichia coli* cells after DpnI digestion, and the resultant mutants were sequence confirmed by DNA sequencing.

Downloaded from https://journals.asm.org/journal/jvi on 12 April 2023 by 147.100.179.233.

CRISPR guide RNA-mediated gene knockout macrophage cell clones. STING$^{-/-}$ and IRF3$^{-/-}$ 3D4/21 cells were previously constructed and used in this study (27). For TBK1 gene knockout, two CRISPR guide RNAs were designed using the Web tool from Benchling, as shown in Table S2 in the supplemental material. The annealed guide RNA encoding DNA sequences was cloned into the BbsI site of pX458-EGFP, and the recombinant pX458-genomic RNA plasmids were sequence confirmed. The 3D4/21 cells grown in 6-well plates (6×10^5 to 8×10^5 cells/well) were cotransfected with two pX458-guide RNA plasmids using Lipofectamine 2000. Twenty-four hours later, the GFP-positive cells were sorted by flow cytometry into 96-well plates for monoclonal cell growth. The individual clones were examined by Western blotting for TBK1 expression and also were analyzed for genomic DNA editing by PCR with the primers shown in Table S2. The genomic PCR products were cloned into T vector using the pClone007 versatile simple vector kit (TsingKe Biological Technology, Beijing, China), and inserted fragments were multiply sequenced. Eight sequences were aligned and analyzed for base indel mutations to ensure the availability of TBK1$^{-/-}$ cell clones.

Promoter-driven luciferase reporter gene assay. 293T cells grown in 96-well plates (3×10^4 cells/well) were cotransfected using Lipofectamine 2000 with ISRE-luciferase reporter or endothelium-leukocyte adhesion molecule (ELAM) (NF-κB)-firefly luciferase (Fluc) reporter (10 ng/well) and β-actin-*Renilla* luciferase (Rluc) reporter (0.2 ng/well), together with the indicated plasmids or the vector control (5 to 40 ng/well). The total DNA per well was normalized to 50 ng by adding corresponding empty vectors. Twenty-four hours after transfection, the cells were lysed, and the Fluc and Rluc activities were measured sequentially with the double-luciferase reporter assay kit. The results were expressed as fold induction of ISRE or ELAM (NF-κB)-Fluc expression, compared with that of vector control, after Fluc normalization by corresponding Rluc values.

RNA extraction, RT, and qPCR. Total RNA was extracted using TRIpure reagent following the manufacturer's suggestions. The extracted RNA was reverse transcribed into cDNA using the HiScript first-strand cDNA synthesis kit, and then the target gene expression levels were measured using qPCR with SYBR qPCR Master Mix (Vazyme Biotech) using StepOne Plus equipment (Applied Biosystems). The qPCR program included a denaturation step at 94°C for 30 s, followed by 40 cycles of 94°C for 5 s and 60°C for 30 s. The relative mRNA levels were normalized to RPL32 mRNA levels and calculated using the $2^{-\Delta\Delta CT}$ method. For PRV-infected cells, the viral loads were determined by TaqMan qPCR. Briefly, total DNA from cells and supernatant was extracted using a DNA extraction kit (Omega, GA, USA). Ten-fold serial dilutions of the PRV-gD plasmid were used to construct a standard curve, on the basis of which the copy numbers of PRV genomic DNA were calculated from the threshold cycle (C_T) values. PCR was performed with the qPCR mix (TaKaRa, Dalian, China) under the following conditions: 95°C for 1 min, followed by 40 cycles of 95°C for 5 s and 60°C for 1 min. The sequences of the qPCR primers and probe used are shown in Table S3 in the supplemental material.

Western blotting. Whole-cell proteins were extracted from cells with radioimmunoprecipitation assay (RIPA) lysis buffer (50 mM Tris [pH 7.2], 150 mM NaCl, 1% sodium deoxycholate, 1% Triton X-100). The protein lysate samples were mixed 3:1 with 4×loading buffer and boiled for 5 to 10 min. The lysate supernatants after centrifugation were run on SDS-PAGE, and then the proteins in the gel were transferred to a polyvinylidene difluoride (PVDF) membrane. The membrane was incubated with 5% skim milk in Tris-buffered saline-Tween 20 (TBST) for 1 h at room temperature, probed with the indicated primary antibodies overnight at 4°C, washed, and then incubated with secondary antibodies for 1 h at room temperature. The protein signals were detected with the enhanced chemiluminescence (ECL) detection substrate and imaging system (Tanon, Shanghai, China).

Plaque assay. Vero cells were seeded into 24-well plates (3×10^5 cells/well), and PK15 cells were seeded into 12-well plates (5×10^5 cells/well). Once the cells were grown into monolayers, the cells were infected with 10-fold serially diluted cell supernatants from HSV-1 (Vero)-, VSV (Vero)-, SeV (Vero)-, or PRV (PK15)-infected cells for 2 h. The infected cells were then washed with phosphate-buffered saline (PBS) and overlaid with an immobilizing medium of a 1:1 mixture of warmed 2×DMEM with 4% FBS and a stock solution of heated 1.6% low-melting-point agarose. Plaque formation took 4 days for HSV-1, 2 days for VSV and SeV, and 3 days for PRV. Upon completion, the immobilizing medium was discarded by tipping, and the cells were fixed and stained with crystal violet cell colony staining solution (0.05% [wt/vol] crystal violet, 1% formaldehyde, 1×PBS, 1% methanol) for 1 h at room temperature. Finally, cells were washed with tap water until the clear plaques appeared. The plaques were counted, and photographs were taken.

$TCID_{50}$ assay. PK15 cells were seeded into 96-well plates (3×10^4 cells/well). After the cells grew into monolayers, the cell medium was removed and the cells were washed twice with PBS. The monolayer cells were infected with 10-fold serially diluted PRV in 1% DMEM. After 3 days of continuous culturing at 37°C, the numbers of wells with and without cell pathogenic effect (CPE) in different treatment groups were recorded, and the viral $TCID_{50}$ values were calculated.

Flow cytometry for apoptosis detection. The level of cell apoptosis was examined using the annexin V-FITC/PI apoptosis detection kit. Briefly, the treated cells were harvested by trypsin digestion, washed with binding buffer, and then resuspended in binding buffer. The staining solutions of annexin V-FITC and PI were added successively. The cells were incubated with fluorescein dyes at room temperature for 15 min in the dark, and the stained cells were immediately detected using flow cytometry. About 10,000 cell events were collected for analysis of FITC and PI signals detected in channels FL1 and FL3, respectively. The FITC and PI signals were processed with FlowJo software and are presented in dot plots.

Downloaded from https://journals.asm.org/journal/jvi on 12 April 2023 by 147.100.179.233.

SUPPLEMENTAL MATERIAL

Supplemental material is available online only.

SUPPLEMENTAL FILE 1, PDF file, 1.5 MB.

ACKNOWLEDGMENTS

The work was partly supported by the National Natural Science Foundation of China (grants 32172867 and 31872450) and a project funded by the Priority Academic Program Development of Jiangsu Higher Education Institutions (PAPD). S.J. was supported by the Postgraduate Research and Practice Innovation Program of Jiangsu Province (Yangzhou University) (grant KYCX21_3272).

We have no financial conflicts of interest.

S. Jiang, N. Xia, J. Luo, Y. Zhang, Q. Cao, J. Zhang, Y. Wang, and Y. Zhao performed the experiments, W. Zheng, N. Chen, F. Meurens, and X. Li contributed to data analysis, and S. Jiang and J. Zhu conceived the idea and wrote the paper.

REFERENCES

1. Takeuchi O, Akira S. 2010. Pattern recognition receptors and inflammation. Cell 140:805–820. https://doi.org/10.1016/j.cell.2010.01.022.
2. Cui J, Chen Y, Wang HY, Wang RF. 2014. Mechanisms and pathways of innate immune activation and regulation in health and cancer. Hum Vaccin Immunother 10:3270–3285. https://doi.org/10.4161/21645515.2014.979640.
3. Dempsey A, Bowie AG. 2015. Innate immune recognition of DNA: a recent history. Virology 479–480:146–152. https://doi.org/10.1016/j.virol.2015.03.013.
4. Sun L, Wu J, Du F, Chen X, Chen ZJ. 2013. Cyclic GMP-AMP synthase is a cytosolic DNA sensor that activates the type I interferon pathway. Science 339:786–791. https://doi.org/10.1126/science.1232458.
5. Jin L, Waterman PM, Jonscher KR, Short CM, Reisdorph NA, Cambier JC. 2008. MPYS, a novel membrane tetraspanner, is associated with major histocompatibility complex class II and mediates transduction of apoptotic signals. Mol Cell Biol 28:5014–5026. https://doi.org/10.1128/MCB.00640-08.
6. Zhong B, Yang Y, Li S, Wang YY, Li Y, Diao F, Lei C, He X, Zhang L, Tien P, Shu HB. 2008. The adaptor protein MITA links virus-sensing receptors to IRF3 transcription factor activation. Immunity 29:538–550. https://doi.org/10.1016/j.immuni.2008.09.003.
7. Ishikawa H, Barber GN. 2008. STING is an endoplasmic reticulum adaptor that facilitates innate immune signalling. Nature 455:674–678. https://doi.org/10.1038/nature07317.
8. Sun W, Li Y, Chen L, Chen H, You F, Zhou X, Zhou Y, Zhai Z, Chen D, Jiang Z. 2009. ERIS, an endoplasmic reticulum IFN stimulator, activates innate immune signaling through dimerization. Proc Natl Acad Sci U S A 106:8653–8658. https://doi.org/10.1073/pnas.0900850106.
9. Zhang C, Shang G, Gui X, Zhang X, Bai XC, Chen ZJ. 2019. Structural basis of STING binding with and phosphorylation by TBK1. Nature 567:394–398. https://doi.org/10.1038/s41586-019-1000-2.
10. Tanaka Y, Chen ZJ. 2012. STING specifies IRF3 phosphorylation by TBK1 in the cytosolic DNA signaling pathway. Sci Signal 5:ra20. https://doi.org/10.1126/scisignal.2002521.
11. Cai X, Chiu YH, Chen ZJ. 2014. The cGAS-cGAMP-STING pathway of cytosolic DNA sensing and signaling. Mol Cell 54:289–296. https://doi.org/10.1016/j.molcel.2014.03.040.
12. Li XD, Wu J, Gao D, Wang H, Sun L, Chen ZJ. 2013. Pivotal roles of cGAS-cGAMP signaling in antiviral defense and immune adjuvant effects. Science 341:1390–1394. https://doi.org/10.1126/science.1244040.
13. Schoggins JW, MacDuff DA, Imanaka N, Gainey MD, Shrestha B, Eitson JL, Mar KB, Richardson RB, Ratushny AV, Litvak V, Dabelic R, Manicassamy B, Aitchison JD, Aderem A, Elliott RM, Garcia-Sastre A, Racaniello V, Snijder EJ, Yokoyama WM, Diamond MS, Virgin HW, Rice CM. 2014. Pan-viral specificity of IFN-induced genes reveals new roles for cGAS in innate immunity. Nature 505:691–695. https://doi.org/10.1038/nature12862.
14. Fang R, Wang C, Jiang Q, Lv M, Gao P, Yu X, Mu P, Zhang R, Bi S, Feng JM, Jiang Z. 2017. NEMO-IKKβ are essential for IRF3 and NF-κB activation in the cGAS-STING pathway. J Immunol 199:3222–3233. https://doi.org/10.4049/jimmunol.1700699.
15. Zheng W, Xia N, Zhang J, Chen N, Meurens F, Liu Z, Zhu J. 2021. How the innate immune DNA sensing cGAS-STING pathway is involved in autophagy. Int J Mol Sci 22:13232. https://doi.org/10.3390/ijms222413232.
16. Gui X, Yang H, Li T, Tan X, Shi P, Li M, Du F, Chen ZJ. 2019. Autophagy induction via STING trafficking is a primordial function of the cGAS pathway. Nature 567:262–266. https://doi.org/10.1038/s41586-019-1006-9.
17. Yamashiro LH, Wilson SC, Morrison HM, Karalis V, Chung JJ, Chen KJ, Bateup HS, Szpara ML, Lee AY, Cox JS, Vance RE. 2020. Interferon-independent STING signaling promotes resistance to HSV-1 in vivo. Nat Commun 11:3382. https://doi.org/10.1038/s41467-020-17156-x.
18. Moretti J, Roy S, Bozec D, Martinez J, Chapman JR, Ueberheide B, Lamming DW, Chen ZJ, Horng T, Yeretssian G, Green DR, Blander JM. 2017. STING senses microbial viability to orchestrate stress-mediated autophagy of the endoplasmic reticulum. Cell 171:809–823.e13. https://doi.org/10.1016/j.cell.2017.09.034.
19. Wu J, Chen YJ, Dobbs N, Sakai T, Liou J, Miner JJ, Yan N. 2019. STING-mediated disruption of calcium homeostasis chronically activates ER stress and primes T cell death. J Exp Med 216:867–883. https://doi.org/10.1084/jem.20182192.
20. Fischer TD, Wang C, Padman BS, Lazarou M, Youle RJ. 2020. STING induces LC3B lipidation onto single-membrane vesicles via the V-ATPase and ATG16L1-WD40 domain. J Cell Biol 219:e202009128. https://doi.org/10.1083/jcb.202009128.
21. Liu D, Wu H, Wang C, Li Y, Tian H, Siraj S, Sehgal SA, Wang X, Wang J, Shang Y, Jiang Z, Liu L, Chen Q. 2019. STING directly activates autophagy to tune the innate immune response. Cell Death Differ 26:1735–1749. https://doi.org/10.1038/s41418-018-0251-z.
22. Ge L, Melville D, Zhang M, Schekman R. 2013. The ER-Golgi intermediate compartment is a key membrane source for the LC3 lipidation step of autophagosome biogenesis. Elife 2:e00947. https://doi.org/10.7554/eLife.00947.
23. Wu J, Yan N. 2022. No longer a one-trick pony: STING signaling activity beyond interferon. J Mol Biol 434:167257. https://doi.org/10.1016/j.jmb.2021.167257.
24. Liu Y, Gordesky-Gold B, Leney-Greene M, Weinbren NL, Tudor M, Cherry S. 2018. Inflammation-induced, STING-dependent autophagy restricts Zika virus infection in the *Drosophila* brain. Cell Host Microbe 24:57–68.e3. https://doi.org/10.1016/j.chom.2018.05.022.
25. Liu Y, Tang Q, Rao Z, Fang Y, Jiang X, Liu W, Luan F, Zeng N. 2021. Inhibition of herpes simplex virus 1 by cepharanthine via promoting cellular autophagy through up-regulation of STING/TBK1/P62 pathway. Antiviral Res 193:105143. https://doi.org/10.1016/j.antiviral.2021.105143.
26. Zhu Q, Hu H, Liu H, Shen H, Yan Z, Gao L. 2020. A synthetic STING agonist inhibits the replication of human parainfluenza virus 3 and rhinovirus 16 through distinct mechanisms. Antiviral Res 183:104933. https://doi.org/10.1016/j.antiviral.2020.104933.
27. Jiang S, Luo J, Zhang Y, Cao Q, Wang Y, Xia N, Zheng W, Chen N, Meurens F, Wu H, Zhu J. 2022. The porcine and chicken innate DNA sensing cGAS-STING-IRF signaling axes exhibit differential species specificity. J Immunol 209:412–426. https://doi.org/10.4049/jimmunol.2101212.

Downloaded from https://journals.asm.org/journal/jvi on 12 April 2023 by 147.100.179.233.

28. Tang CH, Zundell JA, Ranatunga S, Lin C, Nefedova Y, Del Valle JR, Hu CC. 2016. Agonist-mediated activation of STING induces apoptosis in malignant B cells. Cancer Res 76:2137–2152. https://doi.org/10.1158/0008-5472.CAN-15-1885.
29. Wu J, Dobbs N, Yang K, Yan N. 2020. Interferon-independent activities of mammalian STING mediate antiviral response and tumor immune evasion. Immunity 53:115–126.e5. https://doi.org/10.1016/j.immuni.2020.06.009.
30. Yum S, Li M, Fang Y, Chen ZJ. 2021. TBK1 recruitment to STING activates both IRF3 and NF-κB that mediate immune defense against tumors and viral infections. Proc Natl Acad Sci U S A 118:e2100225118. https://doi.org/10.1073/pnas.2100225118.
31. Hopfner KP, Hornung V. 2020. Molecular mechanisms and cellular functions of cGAS-STING signalling. Nat Rev Mol Cell Biol 21:501–521. https://doi.org/10.1038/s41580-020-0244-x.
32. Cai H, Holleufer A, Simonsen B, Schneider J, Lemoine A, Gad HH, Huang J, Huang J, Chen D, Peng T, Marques JT, Hartmann R, Martins NE, Imler JL. 2020. 2′3′-cGAMP triggers a STING- and NF-κB-dependent broad antiviral response in *Drosophila*. Sci Signal 13:eabc4537. https://doi.org/10.1126/scisignal.abc4537.
33. Balka KR, Louis C, Saunders TL, Smith AM, Calleja DJ, D'Silva DB, Moghaddas F, Tailler M, Lawlor KE, Zhan Y, Burns CJ, Wicks IP, Miner JJ, Kile BT, Masters SL, De Nardo D. 2020. TBK1 and IKKε act redundantly to mediate STING-induced NF-κB responses in myeloid cells. Cell Rep 31:107492. https://doi.org/10.1016/j.celrep.2020.03.056.
34. Abe T, Barber GN. 2014. Cytosolic-DNA-mediated, STING-dependent proinflammatory gene induction necessitates canonical NF-κB activation through TBK1. J Virol 88:5328–5341. https://doi.org/10.1128/JVI.00037-14.
35. de Oliveira Mann CC, Orzalli MH, King DS, Kagan JC, Lee ASY, Kranzusch PJ. 2019. Modular architecture of the STING C-terminal tail allows interferon and NF-κB signaling adaptation. Cell Rep 27:1165–1175.e5. https://doi.org/10.1016/j.celrep.2019.03.098.
36. Konno H, Konno K, Barber GN. 2013. Cyclic dinucleotides trigger ULK1 (ATG1) phosphorylation of STING to prevent sustained innate immune signaling. Cell 155:688–698. https://doi.org/10.1016/j.cell.2013.09.049.
37. Hua X, Li B, Song L, Hu C, Li X, Wang D, Xiong Y, Zhao P, He H, Xia Q, Wang F. 2018. Stimulator of interferon genes (STING) provides insect antiviral immunity by promoting Dredd caspase-mediated NF-κB activation. J Biol Chem 293:11878–11890. https://doi.org/10.1074/jbc.RA117.000194.
38. Zhang R, Kang R, Tang D. 2021. The STING1 network regulates autophagy and cell death. Signal Transduct Target Ther 6:208. https://doi.org/10.1038/s41392-021-00613-4.
39. Ablasser A, Goldeck M, Cavlar T, Deimling T, Witte G, Rohl I, Hopfner KP, Ludwig J, Hornung V. 2013. cGAS produces a 2′-5′-linked cyclic dinucleotide second messenger that activates STING. Nature 498:380–384. https://doi.org/10.1038/nature12306.
40. Li S, Yang J, Zhu Y, Ji X, Wang K, Jiang S, Luo J, Wang H, Zheng W, Chen N, Ye J, Meurens F, Zhu J. 2020. Chicken DNA sensing cGAS-STING signal pathway mediates broad spectrum antiviral functions. Vaccines (Basel) 8:369. https://doi.org/10.3390/vaccines8030369.
41. Webb LG, Fernandez-Sesma A. 2022. RNA viruses and the cGAS-STING pathway: reframing our understanding of innate immune sensing. Curr Opin Virol 53:101206. https://doi.org/10.1016/j.coviro.2022.101206.
42. Franz KM, Neidermyer WJ, Tan YJ, Whelan SPJ, Kagan JC. 2018. STING-dependent translation inhibition restricts RNA virus replication. Proc Natl Acad Sci U S A 115:E2058–E2067. https://doi.org/10.1073/pnas.1716937115.
43. Stojdl DF, Lichty BD, tenOever BR, Paterson JM, Power AT, Knowles S, Marius R, Reynard J, Poliquin L, Atkins H, Brown EG, Durbin RK, Durbin JE, Hiscott J, Bell JC. 2003. VSV strains with defects in their ability to shutdown innate immunity are potent systemic anti-cancer agents. Cancer Cell 4:263–275. https://doi.org/10.1016/s1535-6108(03)00241-1.
44. Zheng W, Zhou R, Li S, He S, Luo J, Zhu M, Chen N, Chen H, Meurens F, Zhu J. 2020. Porcine IFI16 negatively regulates cGAS signaling through the restriction of DNA binding and stimulation. Front Immunol 11:1669. https://doi.org/10.3389/fimmu.2020.01669.

Downloaded from https://journals.asm.org/journal/jvi on 12 April 2023 by 147.100.179.233.